Article

Dynamics of Mouth Opening in *Hydra*

Jason A. Carter,[1] Callen Hyland,[1] Robert E. Steele,[3] and Eva-Maria S. Collins[1,2,*]
[1]Division of Biological Sciences and [2]Department of Physics, University of California San Diego, La Jolla, California; and [3]Department of Biological Chemistry and Developmental Biology Center, University of California Irvine, Irvine, California

ABSTRACT *Hydra*, a simple freshwater animal famous for its regenerative capabilities, must tear a hole through its epithelial tissue each time it opens its mouth. The feeding response of *Hydra* has been well-characterized physiologically and is regarded as a classical model system for environmental chemical biology. However, due to a lack of in vivo labeling and imaging tools, the biomechanics of mouth opening have remained completely unexplored. We take advantage of the availability of transgenic *Hydra* lines to perform the first dynamical analysis, to our knowledge, of *Hydra* mouth opening and test existing hypotheses regarding the underlying cellular mechanisms. Through cell position and shape tracking, we show that mouth opening is accompanied by changes in cell shape, but not cellular rearrangements as previously suggested. Treatment with a muscle relaxant impairs mouth opening, supporting the hypothesis that mouth opening is an active process driven by radial contractile processes (myonemes) in the ectoderm. Furthermore, we find that all events exhibit the same relative rate of opening. Because one individual can open consecutively to different amounts, this suggests that the degree of mouth opening is controlled through neuronal signaling. Finally, from the opening dynamics and independent measurements of the elastic properties of the tissues, we estimate the forces exerted by the myonemes to be on the order of a few nanoNewtons. Our study provides the first dynamical framework, to our knowledge, for understanding the remarkable plasticity of the *Hydra* mouth and illustrates that *Hydra* is a powerful system for quantitative biomechanical studies of cell and tissue behaviors in vivo.

INTRODUCTION

Hydra, a freshwater cnidarian polyp, has a morphologically simple body plan with a radially symmetric, tubular body column. *Hydra* is composed of two epithelial layers, the endoderm and ectoderm, which are separated by a layer of extracellular matrix called the mesoglea (1,2). The ectodermal layer is significantly thinner than the endodermal layer, the cells of which are more columnar (3). The apical end of the polyp consists of a ring of tentacles and a dome-shaped hypostome, which contains both the axial organizer and the mouth. The mouth of *Hydra* is a remarkable structure. Unlike in most animals, it is not a permanent opening. Instead, when closed, the *Hydra* mouth is a continuous epithelial sheet, sealed with septate junctions (4–6). The initiation point of mouth opening, however, is conserved between openings and is defined by a morphologically distinct group of cells at the tip of the hypostome (2,5,7,8). The mouth can open wider than the body column during feeding, allowing a *Hydra* polyp to engulf prey larger than itself (5). Other triggers of mouth opening include egestion of indigestible material and osmotic regulation (5,9). The feeding response of *Hydra* can be evoked chemically using reduced glutathione and is regarded as a classical model system for environmental chemical biology (10–13). As such, the behavioral biology of the *Hydra* feeding response has received significant attention, but little is known about the mechanism of mouth opening.

Hydra has a hydrostatic skeleton (14) and its body shape is controlled by longitudinally oriented ectodermal and circularly oriented endodermal epitheliomuscular processes called myonemes (15). Contraction bursts in the ectodermal myonemes are responsible for the spontaneous contraction of the *Hydra* body column in one or more bursts lasting 30–60 s in duration each. These contraction bursts are initiated by electrical impulses from the nervous system (16–18). Because ectodermal myonemes are radially oriented in the hypostome, it has been suggested that they may generate the force for mouth rupture and expansion, while contraction of the antagonistic circularly oriented myonemes in the endoderm would drive closing (19). However, direct experimental evidence for an active expansion of the mouth through myoneme action is lacking. Overall, little is known about the function of myonemes in regulating the behavior of the animal. A recent study (20) implied that the interplay of myonemes in the two epithelial tissues controls the contraction and bending of dissected *Hydra* tissue pieces into a spherical shape during regeneration from small fragments, but the molecular details remain unexplored.

Because large-scale morphological changes often require cell movement, it is conceivable that cellular rearrangements may be necessary to accommodate expansion of the

Submitted June 30, 2015, and accepted for publication January 5, 2016.
*Correspondence: emscollins@ucsd.edu
Jason A. Carter and Callen Hyland contributed equally to this work.
Editor: Jennifer Curtis.
© 2016 by the Biophysical Society
0006-3495/16/03/1191/11
http://dx.doi.org/10.1016/j.bpj.2016.01.008

Hydra mouth, as previously suggested (5). However, one study on an immunocytochemically distinct group of endodermal cells at the tip of the hypostome showed that those cells remained at the rim of the expanding opening (2), suggesting that mouth opening may be achieved via elastic deformation instead of cell displacement. To distinguish between these two possibilities, live imaging of mouth opening and tracking of cell positions during the process is necessary, but requires the availability of transgenic animals and quantitative image analysis. These tools have not previously been available for studies with *Hydra*.

In this study, we employ live imaging of hypostomes in transgenic animals expressing fluorescent proteins in endodermal and ectodermal epithelial cells (21) and quantitative image analysis, to investigate the dynamics of *Hydra* mouth opening for the first time (to our knowledge). We find that the dynamics of mouth opening are on the same timescale as contraction bursts of the *Hydra* body column. Furthermore, using magnesium chloride as a muscle relaxant, we experimentally confirm that mouth opening requires the activity of ectodermal radial myonemes. By tracking individual cells during spontaneous mouth openings we show that cells maintain existing contacts and do not undergo rearrangement. Cell shape analysis further confirms that mouth expansion occurs exclusively through viscoelastic deformation of cells.

Although the degree of mouth opening can vary dramatically between events, we find that all mouth opening events exhibit the same relative rate of opening and that the dynamics are independent of the size or age of the animal. In fact, we observed that individuals can open their mouths consecutively to different amounts, suggesting that the degree of mouth opening is controlled through neuronal signaling.

The expansion of the mouth (area) as a function of time is well described by a modified logistic equation, indicating that mouth opening consists of two phases. In the first phase, the active force exerted by the myonemes increases, leading to accelerated opening. The second phase can be fit by a single exponential, suggesting a passive viscoelastic recoil. Using the relaxation time from the exponential fit and independent measurements of the elastic moduli of the two tissues, we estimate the viscosity to be on the order of 10^4 Pas and the forces required for mouth opening to be on the order of a few nanoNewtons.

This study provides the first dynamical framework, to our knowledge, for understanding the remarkable plasticity of the *Hydra* mouth. We characterize several dynamical and mechanical aspects of mouth opening, which could serve as a starting point for modeling the behavior of two layered tissues bound by extracellular matrix. Importantly, our study illustrates that *Hydra* is a powerful system for biomechanical studies of cell and tissue behaviors in vivo due to the ease of experimental accessibility and the simplicity of the *Hydra* body structure.

MATERIALS AND METHODS

Animal care and transgenic lines

Mass cultures of transgenic *Hydra vulgaris* lines (GFP-ectoderm/DsRed2-endoderm (21) and Wnt3 promoter::GFP (22)) were maintained in *Hydra* culture medium (1.0 mM CaCl2; Spectrum Chemical, Gardenia, CA, and 0.1 mM $MgCl_2$, 0.03 mM KNO_3, 0.5 mM $NaHCO_3$, and 0.08 mM $MgSO_4$; Fisher Scientific, Fairlawn, NJ) using standard procedures (23). Animals were fed three times per week on freshly hatched *Artemia* nauplii (Brine Shrimp Direct, Ogden, UT) and starved for 1–3 days before use in experiments.

Image acquisition

Mouth opening was visualized in transgenic animals using epifluorescence microscopy. Ectoderm and endoderm mouth openings were visualized separately through the use of transgenic *Hydra* expressing GFP and DsRed2 in each tissue layer (21), respectively. For imaging studies, starved animals were decapitated immediately below the tentacles with a scalpel, allowed to heal for at least 2 h, and manually positioned in a drop of *Hydra* medium between two glass coverslips separated by a single layer of double-sided tape. We verified that possible adhesive interactions with the coverslip did not have any observable effect on mouth opening dynamics by comparing mouth opening kinetics of preparations using either cover glass coated with Sigmacote (SL2; Sigma-Aldrich, St. Louis, MO) or bovine serum albumin (BSA; Fisher Scientific) or an uncoated cover glass.

All imaging was performed on a model No. IX81 inverted microscope equipped with a 10×/0.40 UPlanSApo objective, a DSU spinning disk unit (Olympus Optical, Tokyo, Japan), and a Prior ProScan motorized XY stage (Prior Scientific, Rockland, MA). Digital images were captured with an Orca-ER charge-coupled device camera (Hamamatsu Photonics, Shizuoko, Japan) using SlideBook software (Intelligent Imaging Innovations, Denver, CO) running on a Precision 690 PC (Dell, Austin, TX). High-speed, single-channel image sequences of mouth opening were acquired using the camera's streaming mode with a frame rate between 150 and 450 ms. Generally, spontaneous mouth opening events were recorded; however, a feeding response was induced in a subset of experiments by flowing *Hydra* medium containing 0.1 or 0.2 mM reduced L-glutathione (Sigma-Aldrich) into the imaging chamber (5,12). Two-channel movies were recorded using the same approach and equipment, but alternating between GFP and DsRed2 channels throughout the course of a mouth opening sequence, resulting in a slower frame rate of 5.5 s.

Muscle relaxant experiments

We conducted experiments using 2.5% magnesium chloride (wt/vol) in *Hydra* medium on both intact polyps and isolated heads. For mouth opening studies, we performed two different experiments whereby we either (1) mounted the head in *Hydra* medium as described above and induced a feeding response using a solution of 2.5% $MgCl_2$ and 0.2 mM reduced L-glutathione in *Hydra* medium, or (2) mounted the head in 2.5% $MgCl_2$ in *Hydra* medium and induced the feeding response using 0.2 mM reduced L-glutathione in *Hydra* medium alone ($N = 5$ for each condition). For experiments with intact polyps, we recorded the behavior of a polyp ($N = 3$ for *Hydra* medium and $N = 10$ for $MgCl_2$) in *Hydra* medium to a manual squeeze with forceps using a model No. SD6 dissection microscope (Leica Microsystems, Wetzlar, Germany) and model No. A601fc charge-coupled device camera (Basler, Ahrensburg, Germany). Image acquisition was done in MATLAB (The MathWorks, Natick, MA) at five frames per second.

Data analysis

Mouth opening area for both single- and two-channel movies was calculated from binarized images created with a custom adaptive thresholding

algorithm in MATLAB (The MathWorks). In all, 19 ectoderm openings from 14 individual *Hydra* and 15 endoderm openings from 8 individual *Hydra* were recorded using the single-channel method and analyzed using this method. Additionally, nine openings from six individual *Hydra* were taken from two-channel movies and analyzed. The area of mouth opening in each frame was calculated and normalized to the maximum opening size of that opening sequence. As it is difficult to specify the precise moment at which opening begins, areas were aligned at the point of 50% of maximum opening size using a custom MATLAB script. Aligned area values were then binned into 7-s intervals and plotted as a function of time. Therefore, although the beginning and ending of mouth opening are ill defined in terms of absolute time, because they were arbitrarily time-shifted, the shape of the curve remains preserved and thus relative time between events is biologically meaningful.

In the transgenic animals, GFP in the ectodermal epithelial cells is located in the cytoplasm and the nucleus. Because the ectodermal cells contain a large vacuole that displaces the cytoplasm to the perimeter of the cell, it is easy to identify the border of the cell and the nucleus in these cells. Thus, nuclei and cell borders in the ectoderm can be tracked accurately without additional labeling. Eighty individual ectoderm nuclei taken from three individual *Hydra* were selected and manually tracked in every frame throughout mouth opening using ImageJ (National Institutes of Health, Bethesda, MD). Position and time data were recorded in MATLAB. Ectoderm nuclei speeds were calculated and plotted against their instantaneous distance from the center of the mouth. As cell vacuoles are readily visible in endoderm movies while cell nuclei and borders are not, 60 vacuoles from three *Hydra* were tracked and used to calculate cell speeds for the endoderm. In both ectoderm and endoderm movies, the global movement of the mouth was quantified in the same manner described above for cell nuclei and subtracted from the movement of individual cells. All heads used in these experiments were <500 μm in diameter, thus cell speeds were quantified only up to 200 μm from the center of the mouth during opening. Changes in ectoderm cell shape during mouth opening were quantified by manually tracing 55 ectodermal cell borders from six individuals and automatically calculating the aspect ratio by fitting an ellipse to each cell using built-in image analysis methods in ImageJ.

Tissue separation

Methods for separating endodermal and ectodermal tissues were adapted from published protocols (24,25). Body columns were prepared from adult polyps by cutting immediately below the tentacles and above the budding zone with a scalpel. The tissue separation solution consisted of *Hydra* culture medium that was adjusted to pH 2.5 with 2N HCl immediately before use. Body columns were placed in a plastic tube containing separation solution on ice for 2 min and then transferred to a room-temperature hypertonic medium (3.6 mM KCl, 1.2 mM $MgSO_4$, 12.5 mM TES (Fisher Scientific), 6.0 mM $CaCl_2$ (Spectrum Laboratories, Rancho Dominguez, CA), 6.0 mM Na-citrate (LabChem, Zelienople, PA), 6.0 mM Na-pyruvate (Alfa Aesar, Ward Hill, MA), pH 6.9). Within 1–2 min of transfer into hypertonic medium, the ectoderm contracted into a ring and the endoderm into a rod as previously described in Kishimoto et al. (24). The two tissue layers were gently separated from each other using fine forceps and cut into 150–400-μm pieces with a scalpel. Pieces prepared in this manner typically rounded up into spheres within 1–2 h, indicative of their viscoelastic properties. Of note, this is the first time, to our knowledge, that transgenic *Hydra vulgaris* have been used for this kind of tissue separation.

Elastic modulus measurement

The elastic (Young's) modulus (E) of ectodermal and endodermal tissue was determined by parallel plate compression as previously described for zebrafish embryonic tissues (26,27). In brief, a single tissue sphere (consisting of only endoderm or ectoderm) was placed between two parallel plates and a fixed small deformation was applied. The upper compression plate was connected to a model No. D-200 digital recording electrobalance (Cahn, Cerritos, CA) through a nickel-chromium wire to allow measurement of weight (force) changes using MicroScan software (Thermo Electron, Waltham MA). In successive trials, spheres were compressed to various degrees. Tissues were compressed for 10 s, decompressed, and allowed to rest for a few minutes before any subsequent compressions. Plates were coated with either polydimethylsiloxane (PDMS; Ellsworth Adhesives, Germantown, WI) or polyhydroxyethylmethacrylate (poly-HEMA; Sigma-Aldrich, St. Louis, MO) to prevent tissue adhesion. Tissue geometry (deformation) was imaged using a model No. S8 APO dissecting microscope (Leica, Wetzlar, Germany) equipped with a model No. A601f charge-coupled device camera (Basler) and a custom MATLAB image acquisition routine (The MathWorks). The geometry of tissue pieces was analyzed with ImageJ (National Institutes of Health).

Because the cells of both epithelial layers are polarized in the animal, it was possible that they retained some of this polarization leading to internal folds in the tissue spheres that were undetectable with the stereo microscope during tissue compression. Therefore, tissue spheres were checked for folds or pockets of empty space, which would indicate tissue inhomogeneities that could affect the elastic properties by imaging a z-stack on a confocal microscope after compression. Spheres with visible pockets were excluded from further analysis. As small folds and imperfections within the sphere may not be visible, remaining tissue inhomogeneities may contribute to the variability in our measurements. The Young's modulus E was calculated as previously described in Manning et al. (26) using a Hertzian model:

$$E = \frac{3 \times r \times \Delta F_{El}}{4 \times R^3},$$

where r is the original radius of the tissue sphere before compression, F_{El} is the elastic force, and R is the radius of the contact between the tissue sphere and the compression plate. In all, 83 measurements for ectoderm and 88 for endoderm from 17 and 11 individual *Hydra*, respectively, were performed.

RESULTS AND DISCUSSION

The *Hydra* head is composed of a dome-shaped hypostome surrounded by a ring of tentacles (Fig. 1, *A* and *B*). In the center of the hypostome is the mouth, which is sealed with septate cell-cell junctions between a group of anatomically distinct cells when closed (5). The location of the mouth can easily be visualized with phalloidin staining, because actin is a primary component of myonemes and circular myonemes in the endoderm appear as concentric rings with the mouth at the center (Fig. 1, *B* and *C*).

Mouth opening can be triggered experimentally using reduced glutathione (12). In this study, we found that the mouth also opens without external cues or the need of osmotic regulation, as even freshly cut heads that have not yet healed the wound at the aboral end exhibit mouth opening (Movies S1, S2, S3, and S4 in the Supporting Material). We will refer to this opening as "spontaneous mouth opening". While the physiological basis of spontaneous mouth opening remains unclear, a quantitative comparison of the opening dynamics of spontaneous and reduced glutathione-induced opening (Fig. S1, *A–C*; Movie S5) shows that they have similar dynamics. We thus omitted reduced glutathione as a trigger when possible, because spontaneous

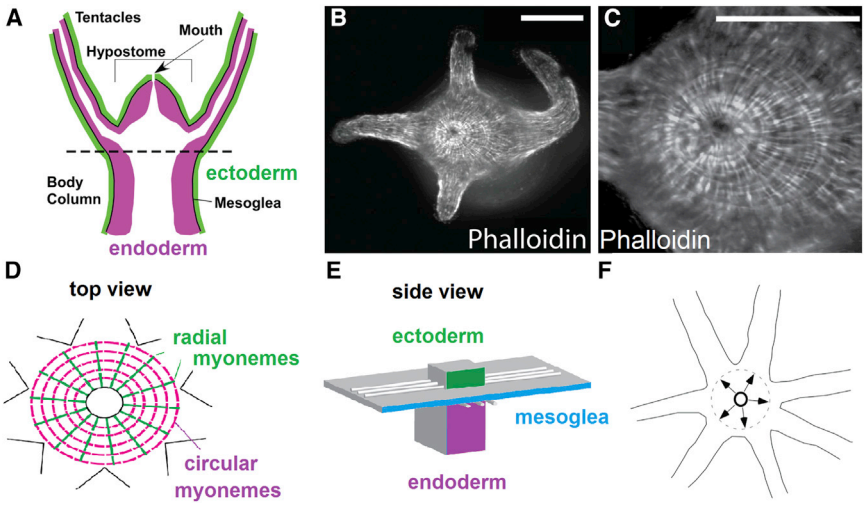

FIGURE 1 The *Hydra* mouth. (*A*) Schematic showing the apical region of *Hydra* in cross section, including ectodermal and endodermal epithelia and mesoglea. (*Dashed line*) Position of head amputation before imaging. (*B*) *Hydra* stained with rhodamine phalloidin to visualize radial and concentric myonemes in ectoderm and endoderm, respectively. (*C*) Higher magnification of hypostome shown in (*B*). Scale bars, 200 μm. (*D*) Top view and (*E*) side view showing orientation of myonemes in the two epithelial layers. Ectodermal myonemes span across several cells while endodermal myonemes, which are perpendicular to the ectodermal ones, are much shorter (28). (*F*) View of the hypostome from above. (*Arrows*) Direction of mouth expansion during opening. (*Dashed line*) Potential maximum opening position of the mouth. To see this figure in color, go online.

mouth opening has the experimental advantage of not requiring chemical or physical perturbations of the sample.

Mouth opening is a myoneme-driven process

The orientation of myonemes in the hypostome (Fig. 1, *B–E*) resembles the orientation of muscle processes in the human iris, where contraction of the radial muscle causes pupil dilation and contraction of the circular muscle causes pupil constriction. Pupil dilation is stimulated by the sympathetic nervous system while pupil constriction is controlled by the parasympathetic nervous system. In *Hydra*, radial and circular myonemes are located in the ectoderm and endoderm, respectively, and each tissue possesses a nerve net (29).

Accordingly, it has been proposed that mouth opening (Fig. 1 *F*) is achieved by active contraction of the ectodermal radial myonemes in response to a signal from the ectodermal nerve net (19). In agreement with this, nerve-free *Hydra* are unable to open their mouths, whether for osmotic regulation or as part of the normal feeding response (30). Furthermore, we found that mouth opening occurs on the same (~60 s) timescale as ectodermal contraction bursts in the body column, which are initiated by electrical impulses from the nervous system (16–18).

To demonstrate directly that myoneme contraction is necessary for mouth opening, we conducted experiments using magnesium chloride and menthol as muscle relaxants, which are commonly used in marine invertebrates (31). Menthol was too harsh on the animals, which disintegrated upon exposure. However, 2.5% (wt/vol) magnesium chloride was found to be an effective relaxant for *Hydra*. While *Hydra* heads exposed to 0.2 mM reduced glutathione readily opened their mouths (Fig. 2, *A–D*; Movie S5), heads exposed to a mixed solution of $MgCl_2$ and 0.2 mM reduced glutathione ($N = 5$) opened the mouth a little bit and then closed again as the *Hydra* head was relaxing (Fig. 2, *E–H*; Movie S6). Similarly, heads that were mounted in 2.5% $MgCl_2$ directly and then exposed to 0.2 mM reduced glutathione did not open their mouths (Fig. 2, *I–L*; $N = 5$). These data suggest that inhibition of myoneme contraction prevents the mouth from opening.

To confirm that magnesium chloride was acting as a muscle relaxant, we also conducted experiments in which we exposed intact *Hydra* polyps to the muscle relaxant. When intact *Hydra* are squeezed with forceps at the upper-half of the body column, they exhibit contraction in response to the stimulus (Movie S7). In agreement with the mouth opening experiments, contraction of the body column in response to a mechanical squeeze with forceps was absent in animals exposed to 2.5% $MgCl_2$ (Fig. S2). In summary, these data argue for ectodermal myoneme contractions being responsible for mouth opening in *Hydra*.

Mouth-opening kinematics

Next, we examined the kinematics of spontaneous mouth opening (Movies S1, S2, and S3). Both ectodermal and endodermal tissue layers were individually imaged throughout the mouth opening process and the area of mouth opening was quantified. Because comparatively little motion takes place along the axis perpendicular to mouth opening (Movie S4), we treat mouth opening as a two-dimensional process in the following analysis.

The exact onset of opening is difficult to determine experimentally. Therefore, opening dynamics were aligned in time by the point at which the area of mouth opening achieved 50% of the maximum opening area (Fig. 3 *A*). This time shift preserves the overall shape of the curve and thus time intervals between events remain biologically meaningful, whereas absolute time in terms of the beginning and ending of mouth opening are arbitrary. The entire opening was complete within ~60 s and the highest rate occurred

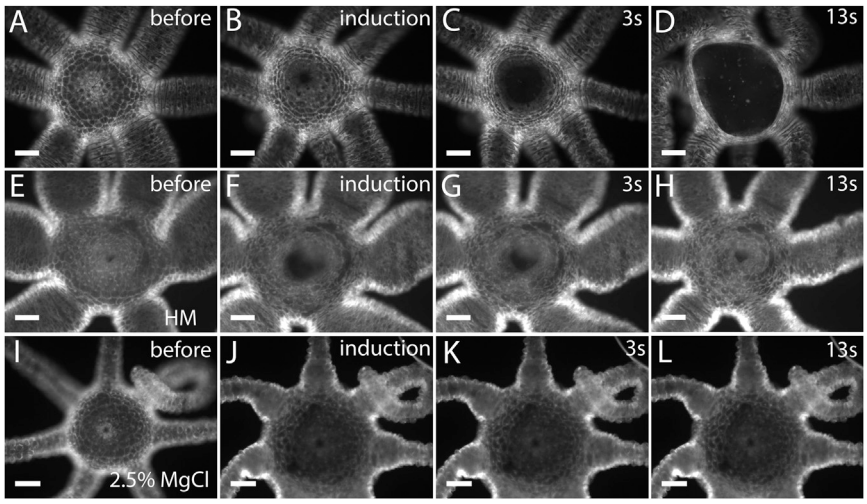

FIGURE 2 Magnesium chloride, as a muscle relaxant, suppresses mouth opening. (*A–D*) Still images from Movie S5 showing the reduced glutathione-induced opening of the ectodermal epithelial layer. The head is mounted in *Hydra* medium and exposed to the stimulant as it is flushed onto the slide. (*E–H*) Still images from Movie S6 showing the reduced glutathione-induced opening of the ectodermal epithelial layer in the presence of 2.5% magnesium chloride (wt/vol). The head is exposed to the stimulant and the relaxant simultaneously as they are flushed onto the slide as a mixture. Although initially mouth opening is activated due to the presence of the reduced glutathione, it quickly closes and relaxes in response to the muscle relaxant. (*I–L*) Still images showing the ectodermal epithelial layer of a *Hydra* head mounted in 2.5% (wt/vol) magnesium chloride in *Hydra* medium. The tentacles appear relaxed and the mouth does not open when the animal is exposed to 0.2 mM reduced glutathione. Scale bar, 100 μm for all images. The exact time of induction of opening is variable due to manual addition of the stimulant.

during the middle-third of the opening. The maximum opening area varied substantially between experiments, with differences between events of up to an order of magnitude (Fig. 3 *A*).

We wondered whether the size or the age of the animal determined the extent of mouth opening, as one would assume that larger and/or more mature animals might possess more or stronger myonemes capable of exerting a larger opening force. To test this, we examined the relationship between the maximum opening area and the size of the head for both ectoderm and endoderm opening. No correlation was found between head size and mouth opening size (Fig. 3 *B*). In addition, heads from buds, i.e., asexual offspring that have not yet separated from the mother polyp and which are significantly smaller than heads from adults, were found to exhibit comparable kinematics and maximum opening areas to adults (Fig. S1, *G–I*; Movie S8). Furthermore, we observed that the same mouth could open multiple times to different degrees within an imaging period (Fig. S3, *A* and *B*). Thus, we conclude that maximum mouth opening area is independent of the size of the *Hydra* head and the age of the animal.

Given the large variability in maximum opening areas, we were surprised to find that normalization of the opening area by the maximum area for each opening sequence caused all curves to collapse to a characteristic sigmoidal shape (Fig. 3, *C* and *D*). This shows that all opening events exhibited the same relative rate of opening and suggests that a neuronal control signal sets the mouth-opening dynamics from the beginning. How neuronal signals are transferred to the ectodermal myonemes, and the spatial dynamics of myoneme activation, are interesting avenues for future research to understand the initial stages of mouth opening.

Because the sigmoidal shape of the normalized mouth opening area versus time curve resembled a logistic curve (Fig. 3 *C*), we fit the time-shifted and normalized ectoderm and endoderm mouth opening area versus time curves (Fig. 3 *C*) with a modified logistic equation (32):

$$A(t) = a + \frac{b}{1 + e^{\left(\frac{-(t-c)}{d}\right)}}, \tag{1}$$

where $A(t)$ is the normalized area of the mouth as a function of time; t is the time from the initiation of the opening process; and a, b, c, and d are fit parameters (Fig. 4). Mathematically, parameter a corresponds to the lower asymptote, b defines the upper asymptote, c is the inflection point (the point at which the sign of the second derivative changes), and d is related to the length of the range of rapid increase (Fig. S4 and Venegas et al. (32)). The results are summarized in Table 1.

Parameters a, b, and c are experimentally constrained and correspond to the initial mouth opening area, the maximum mouth opening area, and the 50% maximum opening, respectively. Given that the *Hydra* mouth is fully sealed when closed, one would expect a to be equal to zero. Similarly, because we fit normalized area curves, we expect b to be equal to 1. Both a and b were determined to have these expected values within the uncertainty of our measurements. Parameter c, in units of time, is the inflection point of the curve and thus the point at which mouth opening begins to slow down. Finally, parameter d, also in units of time, is defined by the points of intersection of a tangent to the A-t curve through the inflection point with the lower and upper asymptotes (Fig. S4 and Venegas et al. (32)). Parameter d is a measure of the steepness of the curve and thus the rate of opening. Together, these four parameters fully capture the kinematics of mouth opening for both tissues separately (Fig. 4, *C* and *D*).

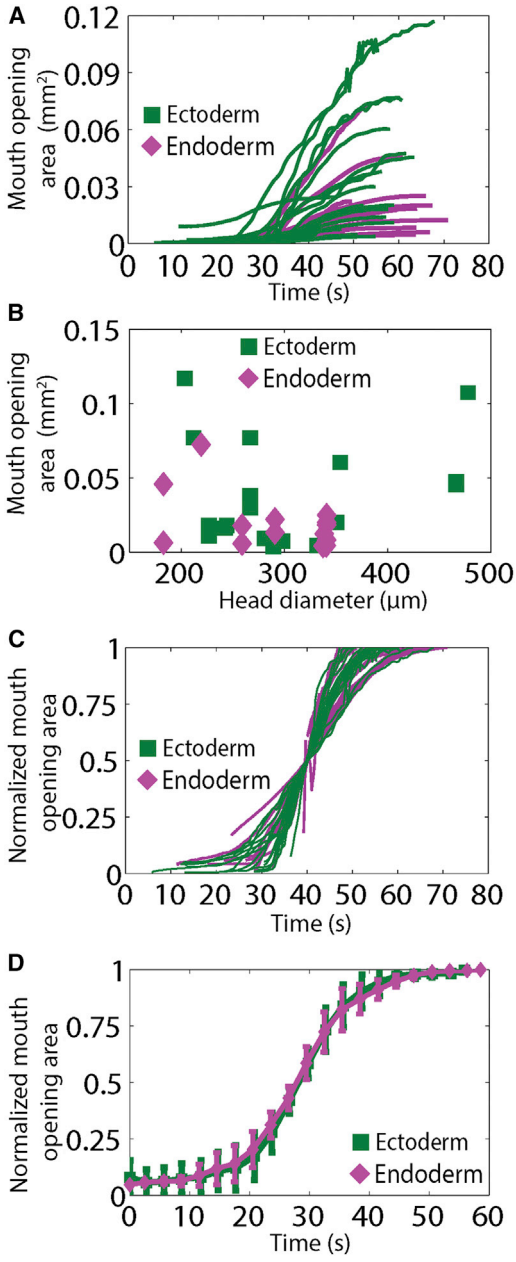

FIGURE 3 *Hydra* mouth opening dynamics. (*A*) Raw opening data for the ectodermal ($N = 19$) and endodermal ($N = 15$) epithelial tissue layers, aligned at the point in time at which the mouth opening area reached 50% of its maximum value. (*B*) No correlation exists between head size and maximum mouth opening area. (*C*) Raw opening data normalized by the maximum opening area show that the relative rate of opening is conserved between animals and independent of the maximum opening. (*D*) Normalized opening data for both ectoderm and endoderm recorded separately from different preparations binned into 7 s intervals and averaged. Error bars denote mean ± SE. To see this figure in color, go online.

The ectodermal layer opens before the endodermal layer

So far we have treated the two epithelial tissues separately, because the data discussed above were collected from independent recordings of the two tissues. However, due to the connection of the two layers through the mesoglea, their dynamics are not independent. Because the radial myonemes responsible for mouth opening (Fig. 2) are located in the ectoderm (see Fig. 1, *D* and *E*) and because the mesoglea, through which these forces are transmitted to the endoderm, is easily stretched, it is conceivable that the ectodermal tissue may begin opening before the endodermal tissue. To test this hypothesis, we acquired two-channel movies of mouth-opening sequences wherein we imaged both tissues of the same animal (Movie S3). Quantitative analysis of these data clearly showed that the ectoderm began to open before the endoderm (Fig. 5, *A–C*). Occasionally it was even observed that while the ectoderm layer underwent partial opening, the endoderm never opened, thus preventing the mouth from opening fully (Movie S9). In addition, we found that the endoderm opened to only ~80% of the ectoderm area at the point of maximum opening (Fig. 5, *A, D*, and *E*). One possible explanation for the difference between maximum ectoderm and endoderm opening size is that the endoderm begins to bulge out through the ectoderm opening at sufficiently large opening areas (Fig. 5 *F*; Movie S4). This bulging of the endoderm was especially pronounced when a feeding response was induced with reduced glutathione (Movie S5).

Because we found that the ectodermal tissue ruptures before the endoderm (Fig. 5, *A–E*), we speculated that the point of maximum acceleration corresponds to the point at which the endoderm starts rupturing as well and both tissue layers are free to fully open together. We quantified the critical threshold area (A_{cr}) of the ectoderm required to induce opening of the endoderm from our two-channel movies (Fig. 4 *A*, *solid line*) and found that A_{cr} is equal to ~15.6% of the maximum opening area, with a standard error of ~3%. Using our sigmoidal fit, the point of maximum acceleration corresponds to (Fig. 4 *A*, *shaded line*):

$$t_a = c - 2d,$$

TABLE 1 Summary of Fit Parameters for Time-Shifted Curves Normalized by the Maximum Opening Area

Fit Parameter	Ectoderm Time-Shifted, Area Normalized	Endoderm Time-Shifted, Area Normalized	Biological Interpretation
a	0.064 (0.056, 0.071)	0.049 (0.038, 0.060)	initial opening area
b	0.93 (0.91, 0.94)	0.95 (0.93, 0.96)	maximum opening area
c (s)	28.7 (28.5, 28.9)	28.3 (28.0, 28.6)	point at which the opening slows down
d (s)	4.20 (4.00, 4.40)	4.97 (4.70, 5.25)	measure of opening rate
R^2	0.9997	0.9994	—

Because we normalize and time-shift, the parameters a, b, and c are the same between ectoderm and endoderm openings. However, there is a difference for parameter d, which is inversely proportional to the rate of opening, between ectoderm and endoderm openings.

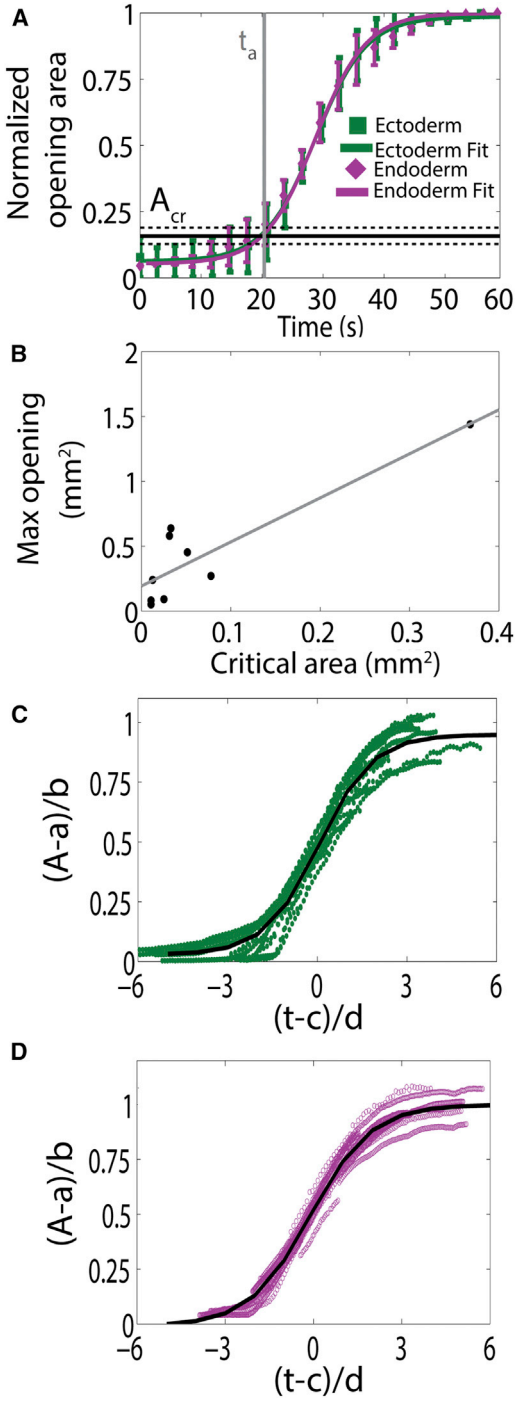

FIGURE 4 Fitting mouth-opening curves. (*A*) Ectoderm and endoderm opening data aligned by 50% of the maximum opening value, binned into 7 s intervals, and fitted according to Eq. 1. The point at which the maximum change in curvature occurs, $t_a = c - 2d$, is shown in shading and the experimentally determined ectodermal critical area (A_{cr}) at which the endoderm begins opening is shown in solid representation. (*Dashed lines*) Mean ± SE of A_{cr}. (*B*) Relationship between the ectoderm critical area and the maximum opening area ($N = 9$). (*C*) Ectoderm ($N = 19$) and (*D*) endoderm ($N = 15$) opening data normalized by fit parameters. (*Solid line*) Population mean. To see this figure in color, go online.

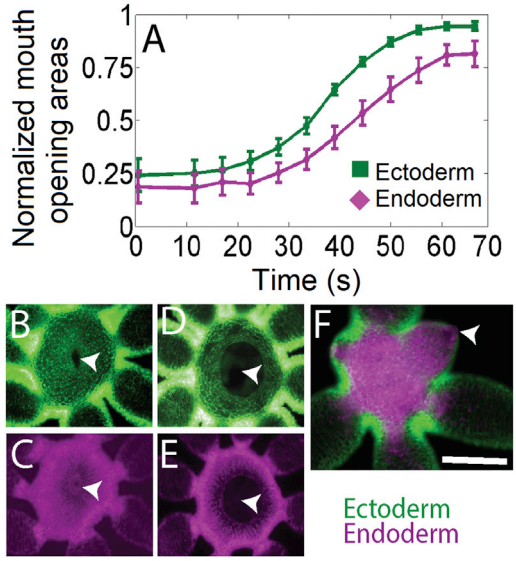

FIGURE 5 Ectoderm opens before endoderm. (*A*) Mouth opening areas for both ectoderm and endoderm from two-channel movies ($N = 9$) were normalized by the maximum opening area of the ectoderm. Plots were shifted to set the ectoderm opening to time zero. Ectoderm mouth opening begins before endoderm opening and the ectoderm ultimately opens more widely than the endoderm. Error bars denote mean ± SE. (*B–E*) Representative images from a two-channel movie showing ectoderm opening has already begun (*B*) while the endoderm remains closed (*C*). (*D* and *E*) Representative images from a two-channel movie showing both ectoderm (*D*) and endoderm (*E*) at the point of maximum opening. (*F*) Representative side-view image from a two-channel movie with ectoderm and endoderm images merged at the point of maximum opening. (*Arrowheads*) Center of the mouth opening. Scale bar, 200 μm. To see this figure in color, go online.

which is when the ectodermal tissue reaches ~15% of its maximum opening area. Thus, the region of maximum acceleration corresponds closely to the point at which the endoderm begins rupturing and mouth opening becomes circularly symmetric (Fig. S5). Furthermore, A_{cr} was found to be directly proportional to the maximum opening area (Fig. 4 *B*). It will be interesting to explore this relationship further and investigate whether a causal connection exists between the critical and maximum opening areas.

Tissue opening dynamics and estimates of their mechanics

As mentioned earlier, parameter d is related to the length of time during which the majority of opening occurs and is thus inversely proportional to the rate of opening. That is, a faster opening corresponds to a steeper area versus time curve and thus a smaller value of d. The observed difference in d between ectoderm and endoderm tissues implies that the two layers open at slightly different rates. One possible explanation for this is that because the force exerted by the ectodermal radial myonemes has to be transmitted to the endoderm through the mesoglea, the endoderm experiences more friction opposing its movement than the ectoderm.

Because the second part of the opening curve and of the velocity curve can be fit by a single exponential (Fig. S6), we can model this part as a damped spring and use the relaxation time τ to check whether there are differences in the viscosity. The relaxation times that we obtain for the two tissues are the same within our measurement uncertainty; for ectoderm, we find $\tau_{ecto} = 7.7(6.4, 9.6)$s and for endoderm, $\tau_{endo} = 7.8(6.9, 8.8)$s, where (x,x) denote the 95% confidence intervals. The fact that τ is the same for both tissues suggests that the observed differences in d must arise from the active part of the curve, because d is obtained from fitting the entire opening curve whereas τ only describes the passive second part. It is an exciting avenue of future research to dissect the biological origin for this difference.

Although the relaxation times measured for the two tissues are identical, the viscosities η could still differ if the tissues possessed different elastic properties, because $\eta = E \times \tau$, where E is the elastic modulus. It is possible to completely separate the two *Hydra* epithelial tissues (Fig. S7, *A–F*) and measure their elastic properties using parallel plate compression (Fig. S7, *G–K*), a technique previously used for measuring the mechanical properties of zebrafish embryonic tissues (26,27). Importantly, both ectoderm and endoderm tissues remain fully viable after separation, as demonstrated by complete *Hydra* regeneration after recombination of separated tissues (Fig. S8). Using compression experiments, we determined the elastic moduli of ectodermal and endodermal tissue spheres to be 4940 ± 563 Pa and 4390 ± 228 Pa (mean ± SE), respectively (Fig. S7, *L* and *M*). These values are comparable to published data on human epithelial cells, which have been reported to have an elastic modulus of ~5 kPa (33). Kücken et al. (34) estimated the elastic modulus of a hollow *Hydra* sphere comprising both tissues and mesoglea to be on the order of 11 kPa, based on studies by Goidin (35). While the elastic properties of isolated *Hydra* mesoglea have not been quantified to the best of our knowledge, the compressive modulus of *Aurelia aurita* jellyfish mesoglea has been reported as tens of kPa (36); thus, our values seem reasonable for the isolated tissues in absence of mesoglea.

The values we measured for the elastic moduli are similar between the two tissues, with ectoderm being only slightly stiffer than endoderm. Thus, the viscosities opposing the movement of the two tissues are basically the same, with $\eta \approx 4 \times 10^4$ Pas, which is comparable to published tissue viscosities of zebrafish embryonic ectoderm and mesendoderm tissues (37).

Mouth opening does not require cellular rearrangement

One of the most detailed studies on *Hydra* mouth opening to date suggested that mouth opening requires cellular rearrangements (5). This hypothesis, however, was never tested experimentally due to lack of appropriate in vivo imaging tools. The ability to perform time-lapse imaging of transgenic *Hydra* polyps with fluorescent epithelial cells enabled us to test whether cell rearrangements play a role in mouth opening (Fig. 6).

As our dynamical analysis of *Hydra* mouth opening has shown that the opening happens in ~60 s (Fig. 4 *A*; Movies S1 and S2), cellular rearrangements are highly unlikely because they would be expected to require a longer timescale. Furthermore, imaging of transgenic *Hydra* expressing GFP under the control of the Wnt3 promotor, which is active in only a small set of cells at the tip of the hypostome (Fig. 6 *A* and Nakamura et al. (22)), revealed that GFP-positive cells remained at the edge of the mouth throughout opening as a continuous rim, indicating that cell rearrangement does not occur (Fig. 6, *B* and *C*). We quantitatively confirmed a lack of cell rearrangement by determining cell trajectories of a subpopulation of cells in the hypostome throughout mouth opening by tracking individual ectodermal cell nuclei throughout mouth opening (Fig. 6, *D–F*). The trajectories of these nuclei clearly show that the relative arrangements of cells are maintained (Fig. 6 *G*).

Cell tracking also allowed us to quantify cell speeds as a function of their distance from the center of the hypostome. We measured the speeds of cell nuclei in the ectoderm and of cell vacuoles in the endoderm (see Materials and Methods) throughout opening. Cells were chosen at various distances from the center, spanning roughly the radius of the hypostome. As expected, the speeds of both ectodermal and endodermal cells decreased as a function of their distance from the center (Fig. 6 *H*).

Because of the substantial tissue deformation that takes place during mouth opening, cells need to either rearrange or deform considerably. As rearrangement does not occur, the change in opening area must be directly reflected in changes in cell shapes, with cells being compressed perpendicularly to the mouth boundary and elongating parallel to it. Indeed, cell-shape changes correlated perfectly with mouth-opening changes and the average aspect ratio of cells doubled from 1.5 to 3 (Fig. 6, *L* and *M*) as quantified through manual tracking of cell morphologies (Fig. 6, *I–K*). Of note, initial mouth opening was not perfectly circular (Fig. S5), indicating local differences in tensions, which were also visually evident in local differences in cell deformations during opening (Fig. 6, *I–K*). As mouth opening progressed, however, asymmetries were less pronounced and the mouth-opening area became more circular (Fig. S5). The origins of the asymmetry are not entirely clear as *Hydra* and its head are thought of as radially symmetric; possible explanations are local differences in the strength of cell-cell junctions or myoneme tension. In summary, our kinematic studies conclusively confirmed that mouth opening is achieved by cell stretching, as proposed by Technau and Holstein (2), and not cell rearrangement, as proposed by Campbell (5).

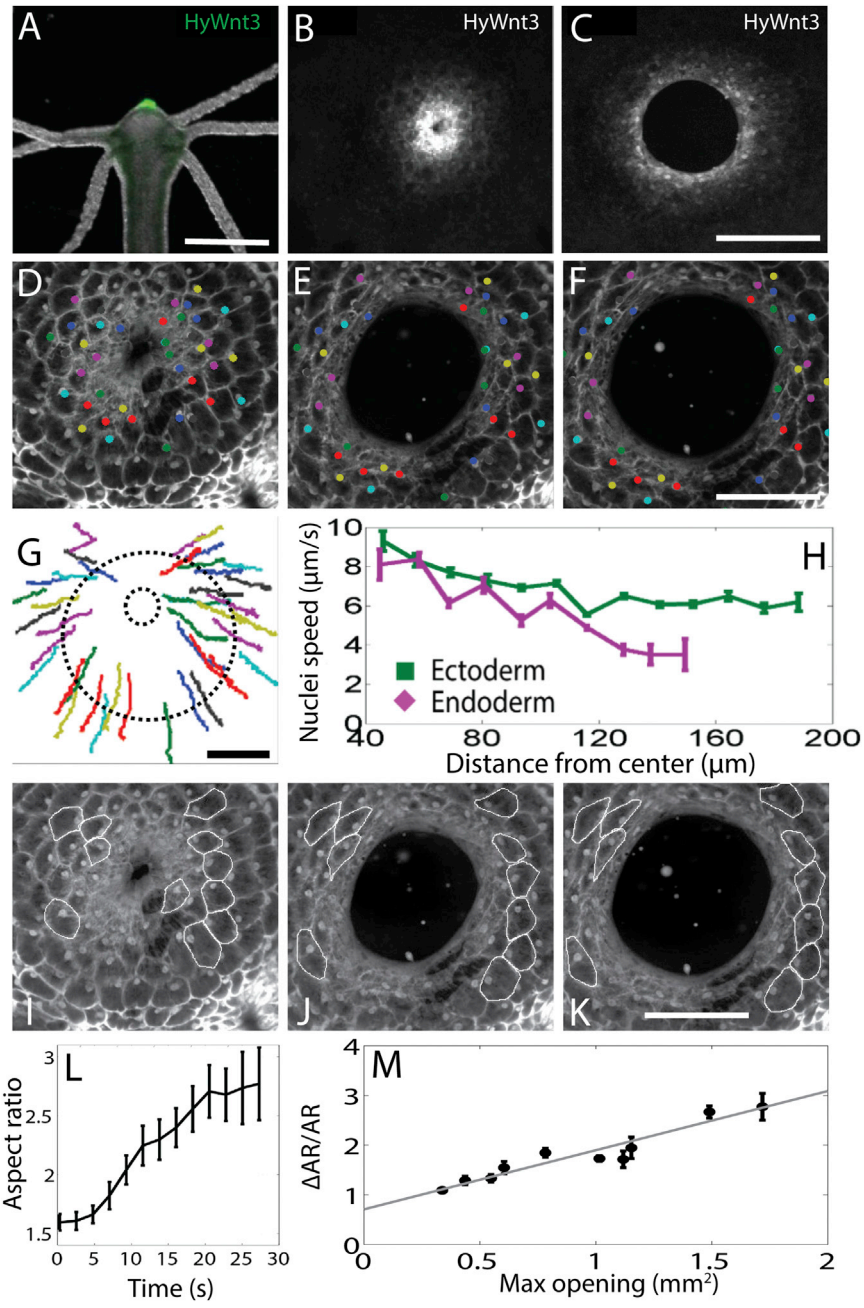

FIGURE 6 Mouth opening involves changes in cell morphology but not cell rearrangement. (*A*) Expression of GFP driven by the Wnt3 promoter is confined to the cells at the tip of the hypostome. (*B*) The mouth of Wnt3 promoter::GFP *Hydra* immediately before mouth opening (0 s) and (*C*) at the point of maximum opening (~40 s). GFP expression remains at the edge of the mouth throughout opening, indicating that cells do not rearrange. (*D–F*) Representative images showing positions of labeled ectoderm nuclei at 0, 15, and 30 s. (*G*) Tracks of individual nuclei recorded every frame for ~40 s through mouth opening show no cell rearrangement. Colors correspond to the same nuclei in each panel. (*H*) Quantification of the speeds of ectoderm cell nuclei ($N = 80$) and endoderm vacuoles ($N = 60$) throughout mouth opening as a function of their distance from the center of the hypostome. The endodermal data are significantly noisier than the ectodermal data because nuclei could not be tracked (see Materials and Methods) and it was difficult to track the position of the vacuoles with the same accuracy as the cell nuclei. (*I–K*) Representative images showing outlines of individual cells at 0, 15, and 30 s of mouth opening. (*L*) Ectoderm cell shapes ($N = 55$) were approximated by the aspect ratio of an ellipse fitted to the cell border. A marked increase in major to minor axis aspect ratio indicates that because cells do not undergo rearrangement, they have to undergo substantial shape changes. (*M*) The maximum opening area of the mouth is directly related to the change in aspect ratio of individual cells ($N = 55$). Error bars indicate mean ± SE. Scale bars, 500 μm in (*A*) and 200 μm in (*C*), (*F*), and (*K*). To see this figure in color, go online.

What are the forces governing mouth opening?

When the mouth is closed, septate junctions connect the central four cells in both epithelial sheets (5). For mouth opening to occur, the opening force must overcome the forces holding both ectoderm and endoderm closed. In the ectoderm, the sealing force is that of the septate junctions, and in the endoderm it is a combination of septate junctions and circularly oriented myonemes. Therefore, mouth opening only occurs when the opening force exceeds the maximum of these closing forces. We do not know the forces required to separate cells held together by septate junctions; however, as an approximation, we can use the forces required to separate two cells sealed by tight junctions, which have been reported to be on the order of a few nanoNewtons (38).

At the point of rupture, mouth opening begins and the net force is equal to the sum of the forces exerted by the radial and circular myonemes. At the inflection point, the opening velocity is maximal (Fig. S6). Beyond that point, the exponential decay allows us to model mouth opening as a damped-spring system. Thus, we can assume that the opening force is constant in the second part of the curve and that increased cell deformation leads to an elastic restoring force opposing further tissue compression. The net force would decrease to zero when these two forces balanced each other and mouth

opening would be maximal. Equating the tissue elastic modulus, E (Fig. S7), with the elastic modulus of single cells assuming tissue confluency, and using the change in aspect ratio of single cells, $\Delta l/L$ (Fig. 6 *L*), we can approximate the required force to reach a desired maximum opening area using

$$F_{El} \approx EA\frac{\Delta l}{L},$$

with F_{El} the elastic force, A the area, Δl the change in radial length, and L the original radial length. This gives a force of ~1–2 nN, which is a reasonable value and on the same order of magnitude as our estimate for breaking septate junctions.

CONCLUSIONS

Taking advantage of transgenic *Hydra* expressing fluorescent proteins in both epithelial layers, we quantified *Hydra* mouth opening kinematics and showed that opening is an active process, mediated by radial myonemes in the ectoderm, and characterized by a sigmoidal mouth area versus time curve. Through cell positional and shape analysis we tested the hypothesis that mouth opening is accompanied by cell rearrangement and showed that cell rearrangement is absent, whereas substantial cell deformation does occur. From the opening dynamics and independent measurements of ectodermal and endodermal elastic moduli we estimated relaxation times and viscosities as well as the forces governing *Hydra* mouth opening. This study provides the first dynamical framework, to our knowledge, for understanding the remarkable plasticity of the *Hydra* mouth. Future experiments on the molecular mechanisms of myoneme control through the nervous system and visualization of myoneme contractions in real-time will allow us to dissect the active part of the mouth opening curve and develop a physical model for the entire mouth opening process. From a more general standpoint, this work illustrates that the structural simplicity and the availability of in vivo labeling techniques make *Hydra* an excellent model for studying fundamental biomechanical processes on both the cellular and tissue levels.

SUPPORTING MATERIAL

Eight figures and nine movies are available at http://www.biophysj.org/biophysj/supplemental/S0006-3495(16)00052-7.

AUTHOR CONTRIBUTIONS

R.E.S. and E.-M.S.C. designed research; C.H. and E.-M.S.C. performed experiments; J.A.C., C.H., and E.-M.S.C. analyzed data. All authors contributed to writing the article.

ACKNOWLEDGMENTS

The authors thank Angel Leu for help with *Hydra* care; Idil Eroglu for help with cell shape tracking; Tiffany Locke, Jannet Cardin, Jennie Nguyen, and Courtney Trinh for imaging mouth opening events; Thomas Holstein for providing the Wnt3 promoter::GFP *Hydra* line; Pat Diamond for discussions, and Olivier Cochet-Escartin and Debbie Yelon for comments on the article.

REFERENCES

1. Bode, H. R. 2009. Axial patterning in hydra. *Cold Spring Harb. Perspect. Biol.* 1:a000463.
2. Technau, U., and T. Holstein. 1995. Head formation in Hydra is different at apical and basal levels. *Development.* 121:1273–1282.
3. Bode, H. R. 2003. Head regeneration in Hydra. *Dev. Dyn.* 226: 225–236.
4. Banerjee, S., A. D. Sousa, and M. A. Bhat. 2006. Organization and function of septate junctions: an evolutionary perspective. *Cell Biochem. Biophys.* 46:65–77.
5. Campbell, R. D. 1987. Structure of the mouth of *Hydra* spp. A breach in the epithelium that disappears when it closes. *Cell Tissue Res.* 249:189–197.
6. Staehelin, L. A. 1974. Structure and function of intercellular junctions. *Int. Rev. Cytol.* 39:191–283.
7. Wood, R. L., and A. M. Kuda. 1980. Formation of junctions in regenerating hydra: septate junctions. *J. Ultrastruct. Res.* 70:104–117.
8. Wood, R. L. 1979. The fine structure of the hypostome and mouth of hydra. II. Transmission electron microscopy. *Cell Tissue Res.* 199:319–338.
9. Benos, D., and R. Prusch. 1972. Osmoregulation in fresh-water Hydra. *Comp. Biochem. Physiol.* 43:165–171.
10. Forrest, H. 1962. Lack of dependence of the feeding reaction in Hydra on reduced glutathione. *Biol. Bull.* 122:343–361.
11. Hanai, K. 1981. A new quantitative analysis of the feeding response in *Hydra japonica*: stimulatory effects of amino acids in addition to reduced glutathione. *J. Comp. Physiol.* 144:503–508.
12. Lenhoff, H. M. 1961. Activation of the feeding reflex in *Hydra littoralis*. I. Role played by reduced glutathione and quantitative assay of the feeding reflex. *J. Gen. Physiol.* 45:331–344.
13. Kulkarni, R., and S. Galande. 2014. Measuring glutathione-induced feeding response in Hydra. *J. Vis. Exp.* 93:e52178.
14. Kier, W. M. 2012. The diversity of hydrostatic skeletons. *J. Exp. Biol.* 215:1247–1257.
15. West, D. L. 1978. The epitheliomuscular cell of Hydra: its fine structure, three-dimensional architecture and relation to morphogenesis. *Tissue Cell.* 10:629–646.
16. Josephson, R. K. 1967. Conduction and contraction in the column of *Hydra*. *J. Exp. Biol.* 47:179–190.
17. Passano, L., and C. McCullough. 1965. Coordinating systems and behaviour in *Hydra*. II. The rhythmic potential system. *J. Exp. Biol.* 42:205–231.
18. Passano, L. M., and C. B. McCullough. 1963. Pacemaker hierarchies controlling the behavior of *Hydra*. *Nature.* 199:1174–1175.
19. Kay, J. C., and G. Kass-Simon. 2009. Glutamatergic transmission in Hydra: NMDA/D-serine affects the electrical activity of the body and tentacles of *Hydra vulgaris* (Cnidaria, Hydrozoa). *Biol. Bull.* 216:113–125.
20. Krahe, M., I. Wenzel, …, C. Futterer. 2013. Fluctuations and differential contraction during regeneration of *Hydra vulgaris* tissue toroids. *New J. Phys.* 15:035004.
21. Glauber, K. M., C. E. Dana, …, R. E. Steele. 2013. A small molecule screen identifies a novel compound that induces a homeotic transformation in Hydra. *Development.* 140:4788–4796.
22. Nakamura, Y., C. D. Tsiairis, …, T. W. Holstein. 2011. Autoregulatory and repressive inputs localize Hydra Wnt3 to the head organizer. *Proc. Natl. Acad. Sci. USA.* 108:9137–9142.

23. Lenhoff, H. M., and R. D. Brown. 1970. Mass culture of Hydra: an improved method and its application to other aquatic invertebrates. *Lab. Anim.* 4:139–154.

24. Kishimoto, Y., M. Murate, and T. Sugiyama. 1996. *Hydra* regeneration from recombined ectodermal and endodermal tissue. I. Epibolic ectodermal spreading is driven by cell intercalation. *J. Cell Sci.* 109: 763–772.

25. Lesh-Laurie, G. 1982. Hydra. *In* Developmental Biology of Freshwater Invertebrates. Alan R. Lis, editor. Bio-Green Books, New Delhi, India.

26. Manning, M. L., R. A. Foty, …, E. M. Schoetz. 2010. Coaction of intercellular adhesion and cortical tension specifies tissue surface tension. *Proc. Natl. Acad. Sci. USA.* 107:12517–12522.

27. Schötz, E. M., M. Lanio, …, M. L. Manning. 2013. Glassy dynamics in three-dimensional embryonic tissues. *J. R. Soc. Interface.* 10:20130726.

28. David, C. 1973. A quantitative method for maceration of hydra tissue. *Wilhelm Roux' Archiv Entwicklungsmech. Organ. J.* 259–268.

29. Davis, L. E., A. L. Burnett, and J. F. Haynes. 1968. Histological and ultrastructural study of the muscular and nervous systems in *Hydra*. II. Nervous system. *J. Exp. Zool.* 167:295–331.

30. Campbell, R. D. 1976. Elimination by Hydra interstitial and nerve cells by means of colchicine. *J. Cell Sci.* 21:1–13.

31. Abrams, M. J., T. Basinger, …, L. Goentoro. 2015. Self-repairing symmetry in jellyfish through mechanically driven reorganization. *Proc. Natl. Acad. Sci. USA.* 112:E3365–E3373.

32. Venegas, J. G., R. S. Harris, and B. A. Simon. 1998. A comprehensive equation for the pulmonary pressure-volume curve. *J. Appl. Physiol.* 84:389–395.

33. Wagh, A. A., E. Roan, …, C. M. Waters. 2008. Localized elasticity measured in epithelial cells migrating at a wound edge using atomic force microscopy. *Am. J. Physiol. Lung Cell. Mol. Physiol.* 295: L54–L60.

34. Kücken, M., J. Soriano, …, E. M. Nicola. 2008. An osmoregulatory basis for shape oscillations in regenerating hydra. *Biophys. J.* 95: 978–985.

35. Goidin, J. 2001. Contributions to a study of morphogenesis in fresh water Hydra. Ph.D. thesis, University of Bayreuth, Bayreuth, Germany.

36. Joshi, K., A. Villanueva, …, S. Priya. 2013. *Aurelia aurita* inspired artificial mesoglea. *Integr. Ferroelectr.* 148:53–66.

37. Schötz, E.-M., R. D. Burdine, …, R. A. Foty. 2008. Quantitative differences in tissue surface tension influence zebrafish germ layer positioning. *HFSP J.* 2:42–56.

38. Vedula, S., T. Lim, …, C. Lim. 2009. Quantifying forces mediated by integral tight junction proteins in cell-cell adhesion. *Exp. Mech.* 49: 3–9.